Journal Européen des Systèmes Automatisés
Vol. 59, No. 7, July, 2026, pp. 2111-2127
Journal homepage: http://iieta.org/journals/jesa

Prescribed-Time Disturbance Observer-Based Sliding Mode Control for Speed Regulation of Permanent Magnet Synchronous Motor Drives

Ali H. Numan[1*], Ashwaq Q. Hameed[2]

[1] Energy and Renewable Energy Department, Electromechanical Engineering College, University of Technology - Iraq, Baghdad 10066, Iraq
[2] Electronic Engineering Department, Electrical Engineering College, University of Technology - Iraq, Baghdad 10066, Iraq

Corresponding Author Email: ali.h.numan@uotechnology.edu.iq

https://doi.org/10.18280/jesa.590725

Received: 7 April 2026
Revised: 11 June 2026
Accepted: 5 July 2026
Available online: 31 July 2026

Keywords:
permanent magnet synchronous motor, prescribed-time control, sliding mode control, chattering elimination, disturbance observer-based control, disturbance estimation, non-vanishing disturbances, time-varying gain

ABSTRACT

This paper proposes a prescribed-time disturbance observer-based sliding mode controller (PT-DOBSMC) for speed regulation of permanent magnet synchronous motor (PMSM) drives within the field-oriented control (FOC) framework. Under the standard assumption of ideal inner current-loop tracking, the PMSM mechanical subsystem reduces to a first-order equation driven by the q-axis current reference and corrupted by an unknown non-vanishing load-torque disturbance. The disturbance is unmeasurable and non-vanishing, which complicates disturbance compensation and chattering reduction simultaneously. A prescribed-time observer (PTO) is therefore introduced to estimate the disturbance before prescribed-time tracking is activated. The PTO employs a time-varying high-gain injection mechanism that achieves asymptotically exact disturbance estimation in the ideal continuous-time model at a user-specified observation deadline. A two-stage sliding mode controller then exploits this property: the first stage maintains bounded speed tracking while the observer converges; the second stage activates a prescribed-time time-varying gain that drives the speed error to zero at a user-chosen tracking deadline. Since the disturbance is exactly cancelled after the observation deadline, the second-stage switching gain is substantially reduced, leading to lower chattering. The control input remains continuous across both stage transitions, preventing impulsive current transients. The observation and tracking deadlines can be selected independently within the proposed framework. Closed-loop stability and prescribed-time convergence are rigorously established via Lyapunov analysis. Simulations under four operating scenarios, including nominal step-speed tracking, deadline-sensitivity studies, and multi-step disturbance rejection, validate the theoretical results and demonstrate improved convergence accuracy and reduced chattering.

1. INTRODUCTION

Permanent magnet synchronous motors (PMSMs) are widely used in high-performance electric drive applications, including electric vehicles, industrial robotics, aerospace actuators, and renewable energy systems [1-3]. Their widespread adoption is attributed to high power density, a wide torque-speed range, and compatibility with the field-oriented control (FOC) framework, which decomposes the nonlinear PMSM dynamics into independently regulated flux and torque channels [4]. Within the FOC architecture, the inner current loops are typically governed by high-bandwidth proportional-integral (PI) controllers or finite-control-set model predictive schemes, while the outer speed loop remains the principal locus of dynamic performance and disturbance rejection [5-7]. It is the behavior of this speed loop under realistic, non-vanishing load disturbances that motivates the present work.

Under the assumption that the inner current loop tracks its reference ideally, a standard and well-validated approximation for drives with fast current dynamics, the PMSM mechanical subsystem reduces to a first-order equation relating rotor speed ω to the q-axis current reference (i_q^*) [8]. The lumped disturbance in this equation is the normalized load torque $d(t) = -\frac{T_l}{J}$, which is genuinely non-vanishing: it persists indefinitely and exhibits time-varying amplitude arising from cutting forces in machine tools, road-gradient variations in traction drives, or wind-gust torques in generator systems [9-11]. Conventional PI speed controllers rely on error accumulation to drive a corrective response, which introduces a fundamental trade-off between bandwidth and disturbance attenuation a trade-off that cannot be resolved by gain tuning alone [12].

Sliding mode control (SMC) is widely employed for disturbance rejection due to its robustness, stemming from the invariance property of the sliding surface and its straightforward implementation within the FOC speed loop [13]. Numerous SMC variants have been developed for PMSM drives. Terminal SMC achieves finite-time convergence; the super-twisting algorithm (STA) reduces chattering while preserving second-order sliding behavior [14], adaptive SMC adjusts the switching gain based on disturbance estimates, and fixed-time SMC-SMO schemes guarantee convergence within a bounded time independent of initial conditions [15]. Despite these advances, a fundamental challenge remains: robust rejection of non-vanishing disturbances requires the switching gain to exceed the disturbance bound, which inevitably increases chattering when disturbances are large. Reducing the gain alleviates chattering but compromises robustness, revealing an inherent limitation of conventional SMC in the absence of disturbance information.

Disturbance observer-based (DOB) control is a commonly adopted approach for addressing this trade-off [16]. The inclusion of a disturbance estimate in the control law as a feedforward compensation term reduces the required switching gain from the disturbance bound to the estimation-error bound, which is typically one to two orders of magnitude smaller. Extended state observers (ESOs), nonlinear disturbance observers (NDOs), and sliding mode observers (SMOs) have all been successfully integrated with SMC for PMSM speed control. A representative recent contribution is, which combines a fixed-time-convergent SMO with a fixed-time SMC, which demonstrates that the switching gain need only bound the observer residual rather than the full disturbance magnitude. A predefined-time DOB combined with adaptive SMC for PMSM was proposed, and a two-stage predefined-time exact SMC framework for generic nonlinear systems appeared in the study [17]. Despite these advances, the following limitation remains: the disturbance estimation error is bounded or converges to zero in finite time, but the convergence instant is either initial-condition dependent or represents only an upper bound, not a user-specified exact deadline.

The prescribed-time control paradigm introduced to overcome precisely this limitation guarantees that all closed-loop errors converge to zero at an exact, user-specified settling time (T^i) regardless of initial conditions and system parameters [18, 19]. This is a strictly stronger guarantee than finite-time control (settling time depends on initial conditions), fixed-time control (settling time is an upper bound), or predefined-time control (actual convergence may precede the predefined instant). Prescribed-time methods achieve this through time-varying feedback gains that grow to infinity as ($t \to T^{i-}$). Significant progress has been made for linear systems [20, 21], nonlinear systems in strict-feedback form [22-24], multi-agent coordination [25-27], and fault-tolerant control [28, 29]. A PTO with time-varying high gain was proposed in the study [30, 31] to achieve zero-error state estimation within a prescribed observation time (T_o), and this observer was used as the foundation of a two-stage backstepping controller for nonlinear systems with non-vanishing disturbances. However, the combination of a prescribed-time zero-error observer with SMC and its application to PMSM speed regulation within the FOC framework remains relatively unexplored.

When the disturbance estimation error converges to zero by (T_o), the Stage-2 scheme performs disturbance estimation and prescribed-time tracking separately at different stages, and the two stages are prescribed with different time limits. This separation leads to a two-timescale architecture: The observer is used first, before the high-gain tracking phase kicks on, so the prescribed-time SMC gain acts on a disturbance-free plant, and chattering elimination is a structural property of the design, and not just an approximation.

The novelty of the proposed prescribed-time disturbance observer-based sliding mode controller (PT-DOBSMC) method can be summarized as follows:

1. The existing "fixed-time" and "predefined-time" observer-based controllers usually can ensure that the estimation error satisfies boundedness or convergence to an arbitrarily small residual at the end of the period. Unlike the PTO in existing literature, however, the proposed one is designed with a time-varying high-gain injection mechanism that can make the estimation error converge to exactly zero at a user-specified observation deadline (T_o).

2. The traditional SMC for chattering elimination (e.g., adaptive SMC or observer-based SMC) usually needs a switching gain to be large enough to cover the residual error of the observer. Our two-stage controller is able to achieve exactly the cancellation of disturbance by reducing the switching gain in the second stage ($t \geq T_o$) to a negligible level.

3. The framework of the proposed method is based on two independent prescribed deadlines: observation deadline (T_o) and tracking deadline (T_f). This enables the designer to independently adjust the disturbance rejection speed and tracking performance. This is not the case in most single-stage prescribed time controllers, i.e., observer and controller convergence are often linked.

4. The suggested approach explicitly solved the problem of having C^p continuity of the control input from stage to stage (T_o and T_f). Impulsive current transients at switching stages have often been a problem in this field in the past. Still, the proposed gain structuring method provides a smooth and continuous transition, avoiding the loading or stress on the power electronics, which is crucial for practical applications of PMSM drives.

The DOB and ESOs can only ensure asymptotic (fixed-time) convergence, which entails some estimation error and high, persistent switching gains for the controller and chattering phenomenon. The PTO, on the other hand, forces the disturbance estimation error to converge to zero at a user-defined time (T_o) for any initial condition and disturbance magnitude. This makes the switching gain of the controller much smaller for eliminating the chattering phenomenon in the structure. Furthermore, it offers two timescale tunings, where one can independently tune the observation deadline (T_o) and tracking deadline (T_f) to adjust the speed of disturbance rejection and the transient tracking performance without risking impulsive current transients.

Motivated by the above, this paper proposes a PT-DOBSMC strategy for PMSM speed regulation within the FOC framework. The speed tracking error serves as the sliding variable, and the q-axis current reference is the control input. A PTO with a time-varying high gain is designed to achieve zero-error disturbance estimation at exactly the prescribed observation time (T_o).

1. A prescribed-time DOB is developed for PMSM speed regulation within the FOC framework. Unlike predefined-time and fixed-time observers, which achieve only a bounded estimation error at the observation deadline, the proposed observer drives the estimation error to zero at a user-specified observation instant.

2. A two-stage sliding mode controller is proposed. The first stage maintains bounded speed tracking while the observer converges to the disturbance. The second stage activates after

the observation deadline and drives the speed error to zero at a user-specified tracking deadline. The switching gain in the second stage is substantially reduced compared to the first stage, resulting in reduced chattering.

3. The transition between the two control stages is proven to be continuous. No impulsive current commands arise at either stage boundary, which protects the power electronics from stress associated with abrupt current changes. The two prescribed deadlines, one for observation and one for tracking, are independently selectable by the designer and do not depend on initial conditions or load magnitude.

4. The proposed strategy is evaluated using MATLAB/Simulink simulations under four different operating conditions. The results demonstrate the efficacy of the developed strategy with reduced chattering.

The limitations of the fixed-time, predefined-time and extended state observer-based approaches are overcome with the proposed PT-DOBSMC framework, which has a convergence time that is independent of initial system conditions and/or conservative upper bounds, or chattering due to high switching gains. The framework addresses these challenges by separating the process of observing and tracking in user-specific (T_o and T_f) deadlines. In particular, the time-varying high-gain injection mechanism, which has a decay-stabilization term, forces the disturbance estimation error to go to zero exactly at (T_o). This exact alignment allows the structural reduction of the Stage-2 sliding mode switching gain (ρ_{sw2}) to an arbitrarily small value, which fundamentally makes chattering disappear.

The remainder of this paper is organized as follows. Section 2 formulates the PMSM control problem and defines the disturbance exosystem model. Section 3 describes the PTO design and proves zero-error convergence. Section 4 develops the proposed two-stage PT-DOBSMC framework and analyses its stability. Section 5 reports the simulation results, and Section 6 concludes the paper.

2. PROBLEM FORMULATION AND CONTROL ARCHITECTURE

2.1 Permanent magnet synchronous motor mechanical subsystem under ideal field-oriented control

The complete PMSM model in the synchronously rotating d--q reference frame includes coupled electrical dynamics and a mechanical equation. Within the FOC paradigm, the direct-axis current reference is set to zero (maximum-torque-per-ampere for surface-mounted PMSM), and torque is regulated exclusively through (i_q^*). This paper adopts the standard well-justified assumption that the inner current loops track their references without dynamic error — an approximation that holds whenever the current-loop bandwidth exceeds the speed-loop bandwidth, which is typical in industrial drives. Under this assumption, the PMSM mechanical subsystem reduces to a first-order nonlinear system.

$$\dot{\omega} = K_{t\prime}\, i_q^* - b\omega + d(t) \tag{1}$$

where, the system parameters are defined as $K_{t\prime} = \frac{K_t}{J}$, $b = \frac{B}{J}$. The K_t and B are the motor torque constant and viscous friction coefficient, respectively, and J is the rotor inertia. The nominal parameter values ($\hat{K}_t'$, $\hat{b}$) are used during the design of the controller, and any variation or uncertainty of the motor parameters (such as changes in the rotor inertia (ΔJ), viscous friction coefficient (ΔB) or torque constant (ΔK_t) will be included in the total non-vanishing disturbance term $d(t)$:

$$d(t) = -\frac{T_L}{J} + \left(K_t' - \hat{K}_t'\right) i_q^* - (b - \hat{b})\omega \tag{2}$$

Due to the nature of the proposed PTO, variations of all the parameters (J, B, K_t) are continuously estimated, suppressed, and transmitted to the user-defined observation time (T_o).

It is assumed in this study that the inner current-loop tracking is ideal. The finite current-loop bandwidth effect is common in DC motor high performance texts, but is discussed in Section 6 with regard to practical robustness.

2.2 Structured non-vanishing disturbance model

Rather than treating $d(t)$ as a merely bounded signal, a common assumption that unnecessarily inflates SMC switching gains and chattering, this paper adopts an exosystem-based model: the disturbance is assumed to be generated by an unknown but finite-dimensional autonomous linear system,

$$\begin{gathered} \dot{\sigma_r} = \sigma_{r+1}, r = 1, \dots, m-1 \\ \dot{\sigma_m} = \sum_{r=1}^{m} b_r \sigma_r \\ d(t) = \sigma_1(t) \end{gathered} \tag{3}$$

An autonomous linear exosystem structure is used here because of the significant spectral flexibility and ease of use in modeling typical load-torque perturbations with PMSM. In particular, the most relevant disturbance classes of high-performance electric drives, such as constant load torque ($m = 1, b_1 = 0$), periodic cogging torque and eccentricity ($m = 2$), and the ramp-type disturbances resulting from the slow change in speed ($m = 2, b_1 = 0$), are explicitly covered in this formulation. The formulation of the disturbance as a solution to a finite-dimensional autonomous linear system is an important step since it allows for modeling the time-varying nature of these real-world phenomena. This model provides the basis for the disturbance estimation procedure developed in Section 3.

2.3 Standing assumptions

Assumption 1: The speed reference ω_{ref} and its time derivatives continuous and uniformly bounded for all $t \geq 0$.

Assumption 2: The disturbance $d(t)$ is generated by the exosystem (3) with unknown parameters (b_r) and known structural order m. The initial state of the exosystem is bounded but otherwise unknown. These two assumptions are standard in observer-based disturbance compensation literature [32, 33] and are satisfied by any load torque that can be represented, at the least locally, as a solution of a linear ordinary differential equation (ODE).

2.4 Two-timescale prescribed-time control objective

Unlike many existing PMSM speed-control approaches, the proposed framework explicitly partitions the closed-loop objective into two independent prescribed deadlines — an observation deadline and a tracking deadline — each freely assigned by the designer independent of initial conditions. Define the speed tracking error and the sliding variable identically as

$$e(t) = \omega_{ref}(t) - \omega(t), \; s(t) = e(t) \tag{4}$$

The control objective is threefold. First, the disturbance estimation error must vanish exactly at the prescribed observation time ($T_o > 0$):

$$\tilde{d}(t) \triangleq d(t) - \hat{d}(t) \equiv 0, \; \forall \, t \geq T_o \tag{5}$$

Second, the speed tracking error must vanish exactly at the prescribed tracking time ($T^i > T_o$), and the control input must remain within the inverter current rating throughout:

$$e(t) \equiv 0, \forall t \geq T_f \tag{6}$$

$$|i_q^*(t)| \leq i_{q,max}, \forall t \geq 0$$

Third, all closed-loop signals must be continuous and bounded for all ($t \geq 0$), and the control input ($i_y^*(t)$) must be (C^n) continuous at both (T_o) and (T^i) a requirement that rules out impulsive current transients at the stage-switching instants and that has not been explicitly addressed in any prior PMSM prescribed-time or predefined-time control work. The separation ($T_o < T^i$) creates a two-timescale architecture: the observer completes its task before the high-gain tracking phase activates, so the prescribed-time SMC gain ($\psi_0(t)$) operates on a disturbance-free plant, and chattering elimination becomes a structural property of the design rather than an approximation. The observer and controller realizing objectives Eqs. (5) and (6) are derived in Sections 3 and 4, respectively. The proposed PT-DOBSMC for speed regulation of PMSM drives is shown in Figure 1.

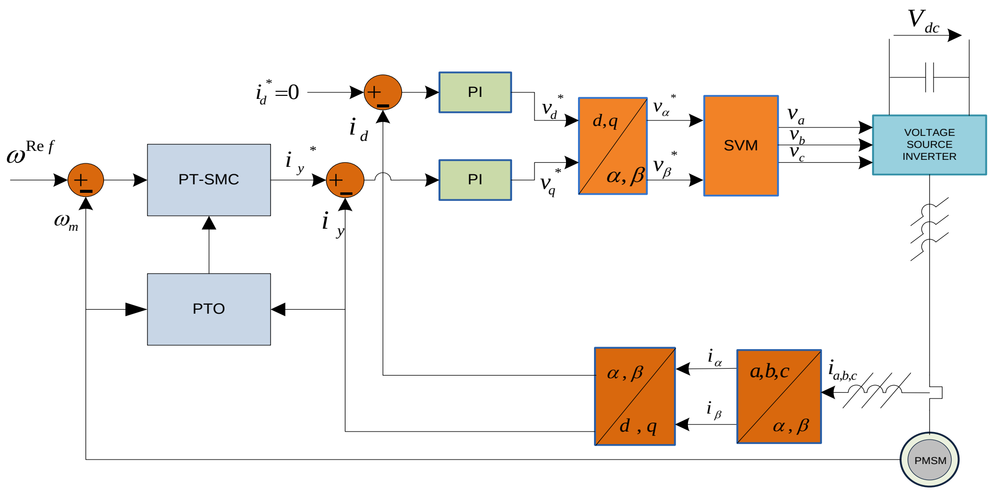

Figure 1. Proposed prescribed-time disturbance observer-based sliding mode controller (PT-DOBSMC) strategy for speed regulation of permanent magnet synchronous motor (PMSM) drives

3. PRESCRIBED-TIME OBSERVER DESIGN

To achieve objective Eq. (5), the disturbance estimation problem is reformulated through a coordinate transformation. The standard approach to designing an asymptotic observer and accepting a bounded residual is incompatible with the objective of exact zero-error at a user-specified deadline. Instead, we exploit the finite-dimensional exosystem structure of (3) through a coordinate transformation that converts the disturbance estimation problem into a linear observer canonical form, and then inject a time-varying gain that grows to infinity at exactly (T_o) to enforce exact convergence. An additional decaying term in the gain ensures that the error remains at zero after (T_o), without any persistent high gain — a property absent from fixed-time and predefined-time observers.

3.1 Known composite driving term

Before constructing the observer, it is useful to isolate the portion of the plant dynamics that is fully known at every instant. Substituting Eqs. (1) and (2), the composite term is:

$$\varphi(t) = K_{t},i_q^* - b \tag{7}$$

This equation is computable in real time from the measured speed ω and the commanded current reference (i_y^*). The term ($\varphi(t)$) plays the role of a known input to the observer, and the entire observer design proceeds without requiring knowledge of the exosystem parameters (b_r).

3.2 Coordinate transformation and transformed dynamics

To convert the coupled plant–exosystem into an observable canonical form, we introduce the following state transformation that absorbs the coupling between the mechanical state ω and the exosystem outputs:

$$\begin{gathered} \xi_1 = \omega \\ \xi_2 = d - b_m\omega \\ \xi_k = d^{(k-2)} - b_m d^{(k-3)} - \cdots - b_{m-k+2}\omega, \\ k = 3, \ldots, m+1 \end{gathered} \tag{8}$$

Transformation Eq. (8) avoids repeated differentiation of exosystem states, which eliminates the complexity explosion that afflicts backstepping-based observer schemes [34]. Differentiating Eq. (8) along the trajectories of Eqs. (1) and

(3), and using Eq. (7), the transformed states (ξ_k) evolve as

$$\begin{gathered}\dot{\xi_1} = \xi_2 + b_m\omega + \varphi \\ \dot{\xi_k} = \xi_{k+1} + b_{m-k+1}\omega - b_{m-k+2}\varphi, k = 2, \ldots, m \\ \dot{\xi}_{m+1} = -b_1\varphi\end{gathered} \tag{9}$$

System Eq. (9) is driven entirely by the known term ($\varphi(t)$) and the measurable speed ω; the unknown exosystem parameters (b_r) appear only as coefficients of known quantities. This property results in linear estimation-error dynamics, which are amenable to prescribed-time design.

3.3 Prescribed-Time Observer equations and linear error dynamics

The PTO mirrors the transformed dynamics Eq. (9) with output-injection terms driven by the measurable error in the first transformed state ($\xi_1 = \omega, so\ \xi_1$ - $\hat{\xi}_1$ = ω - $\hat{\xi}_1$ is directly observable):

$$\begin{gathered}\dot{\hat{\xi}}_1 = \hat{\xi}_2 + b_m\omega + \varphi + \rho_1(\omega - \hat{\xi}_1) \\ \dot{\hat{\xi}}_k = \widehat{\xi_{k+1}} + b_{m-k+1}\omega - b_{m-k+2}\varphi + \rho_k(\omega - \hat{\xi}_1), \\ k = 2, \ldots, m \\ \dot{\widehat{\xi_{m+1}}} = -b_1\varphi + \rho_{m+1}(\omega - \hat{\xi}_1)\end{gathered} \tag{10}$$

Subtracting the observer dynamics Eq. (10) from the plant dynamics Eq. (9) causes the unknown $d(t)$ and the exosystem parameters (b_r) to be explicitly canceled and leaves the error system Eq. (11) linear and independent of the disturbance. The observation errors ($e_k = \xi_k - \hat{\xi}_k$) satisfy a system that takes the linear form:

$$\begin{gathered}e_k = \xi_k - \hat{\xi}_k, k = 1, \ldots, m+1 \\ \dot{e_1} = e_2 - \rho_1 e_1 \\ \dot{e_k} = e_{k+1} - \rho_k e_1, k = 2, \ldots, m \\ \dot{e}_{m+1} = -\rho_{m+1}e_1\end{gathered} \tag{11}$$

The error system Eq. (11) is linear in e and completely free of the unknown parameters (b_r) — they canceled exactly in the subtraction. This linearity results from the coordinate transformation Eq. (8), which allows (ρ_k(t)) to be designed purely from the desired error polynomial, independent of the disturbance. The equations in Eq. (11) are written in matrix form ($\dot{e} = \Lambda(t)e$), with the companion matrix given as:

$$\bar{\Lambda} = \begin{bmatrix} -p_1 & 1 & 0 & \cdots & 0 \\ -p_2 & 0 & 1 & \cdots & 0 \\ \vdots & \vdots & \vdots & \ddots & \vdots \\ -p_m & 0 & 0 & \cdots & 1 \\ 0 & 0 & 0 & \cdots & 0 \end{bmatrix} \in R^{(m+1)\times(m+1)} \tag{12}$$

The designer chooses the coefficients (p_k) such that the polynomial ($s^m + p_1 s^{m-1} + \cdots + p^m$) is Hurwitz. For the PMSM case with ($m = 1$), the stability condition simplifies to ($p_1 > 0$), which requires only a positive observer pole.

3.4 Time-varying prescribed-time injection gains

Zero-error convergence is achieved through the time-varying scaling function ($\mu(t)$), which grows without bound as ($t \to T_o{}^-$):

$$\begin{gathered}\mu(t) = \frac{T_o}{T_o - t}, 0 \le t < T_o \\ \mu(t) = 0, t \ge T_o\end{gathered} \tag{13}$$

As ($t \to T_o{}^-$), ($\mu(t) \to +\infty$), and this causes the injection gains to increase and enforce convergence at the prescribed instant. After (T_o) and (μ) are set to zero, and the gains vanish, which releases the observer from the high-gain regime. For the two-state case (m = 1), the gains take the explicit form:

$$\begin{gathered}\rho_1(t) = (2\alpha\mu + T_o - t)\alpha^2, t < T_o \\ \rho_2(t) = \alpha^2\mu^2, t < T_o \\ \rho_k(t) = 0, t \ge T_o, k = 1,2\end{gathered} \tag{14}$$

Here ($\alpha > 0$) is the single tuning parameter that sets the error convergence rate: the error characteristic polynomial becomes $(s + \alpha\mu)^2$, whose roots track ($-\alpha\mu$ to $-\infty$) as ($t \to T_o^-$). The term ($T_o - t)\alpha^2$ in (ρ_1) is the "v-term" introduced in the study [26]: This is a decay-stabilization contribution that vanishes precisely at (T_o) , thereby ensuring a smooth transition from the regime ($t < T_o$) to ($t \ge T_o$), as well as perfect continued tracking by the observer even after the injection gains have reduced to zero. For numerical robustness, a cap ($\rho_k \le \rho^{max}$) is imposed in the final moments before (T_o); since the error is already vanishingly small at that point, the cap does not affect the theoretical guarantee.

3.5 Disturbance estimate recovery

The disturbance is estimated by inverting the coordinate transformation given in Eq. (8) after the computation of the observer states ($\hat{\xi}_k$). From the definition ($\xi_2 = d - b^m\omega$), solving for d gives:

$$\begin{gathered}\hat{d}(t) = \hat{\xi}_2 + b_m\omega(t) \\ \hat{d}(t) = \hat{\xi}_2[m = 1]\end{gathered} \tag{15}$$

For the practically important case (m = 1) with a constant load torque model (b_1 = 0), the recovery simplifies to $(\widehat{d} = \hat{\xi}_2)$ — the observer's second state directly carries the disturbance estimate, without any additional computation. Higher-order exosystems (m = 2 for sinusoidal loads, m = 3 for the simulation example in Section V) require the full recovery formula but add no structural complexity; only the observer dimension increases.

3.6 Main convergence result

This section is intended to state the main result formally.

Theorem 1 (Prescribed-Time Zero-Error Convergence): Let Assumption 2 hold and let the observer gains ($\rho_k(t)$) be given by Eq. (14) [or its general-m counterpart], with ($\alpha > 0$) chosen such that the polynomial ($s^m + p_1 s^{m-1} + \ldots + p^m$) is Hurwitz. Then the observation errors ($e_k(t) = \xi_k - \hat{\xi_k}$) satisfy: (i) $|e_k(t)|$ is bounded for all $t \in (0, T_o)$; (ii) ($e_k(t) \to 0$) as ($t \to T_o^-$) ; and (iii) ($e_k(t) \equiv 0$) for all ($t \ge T_o$) , provided the disturbance trajectory continues to be generated by the same exosystem realization that was active during $[0, T_o]$. Consequently, ($\hat{d}(t) = d(t)$) for all ($t \ge T_o$) in the ideal continuous-time setting, subject to the same proviso.

Proof: Consider the Lyapunov candidate for the error system Eq. (11):

$$V_e = \frac{1}{2}e^T e = \frac{1}{2}\sum_{k=1}^{m+1} {e_k}^2 \tag{16}$$

where, $(P > 0)$ is the unique solution to the matrix Lyapunov equation:

$$\bar{\Lambda}^T P + P\bar{\Lambda} = -2I \tag{17}$$

which exists since $(\bar{\Lambda})$ is Hurwitz. Define $\left(\kappa = \frac{1}{\lambda_{max}(P)} > 0\right)$, so that $(e^T e \geq 2\kappa V_e)$ by the Rayleigh quotient. The central step is to show that the gain structure Eq. (14) produces the decomposition:

$$\Lambda(t) = \mu(t) \cdot \bar{\Lambda} + R(t) \tag{18}$$

where, $\|R(t)\| = O(T_o - t) \to 0$ as $(t \to T_o)$. This holds because each gain $(\rho_k(t))$ in Eq. (14) splits as $(\rho_k(t) = \mu.(\bar{\Lambda}\ entery) + (T_o - t).\rho_k)$; the first term produces the $(\mu\bar{\Lambda})$ factor, the second is the v-term and forms $R(t)$. The Lyapunov derivative is dominated by the (-2μ) term as (t) approaches $(t \to T_o^-)$, from below, so the residual matrix $R(t)$ is negative definite for all (t) close to $(t \to T_o^-)$ and for all $(t \to T_o^-)$, because the deviation of the time-varying gain from the prescribed-time structure is dominant. Differentiating (V_e) along Eq. (11) and substituting:

$$\begin{aligned}\dot{V}_e &= \frac{1}{2}e^T\big(\Lambda(t)^T P + P\Lambda(t)\big)e \\ &= \frac{1}{2}e^T[\mu(\bar{\Lambda}^T P + P\bar{\Lambda}) + R(t)^T P + PR(t)]e \\ &= \frac{1}{2}e^T\big(-2\mu I + R(t)^T P + PR(t)\big)e \\ &\leq -2\kappa\mu(1 - c\|R\|/\mu)V_e \leq -2\kappa\mu V_e\end{aligned} \tag{19}$$

The last inequality uses $(e^{\mathrm{T}}e \geq 2\kappa V_{\mathrm{e}})$ and the bound $(\mathrm{c}\|R\|/\mu = O((T_o - t)^2/T_o) \to 0)$, confirming Eq. (19) is a strict inequality throughout $(0, T_o)$. where (κ) Integrating Eq. (19) using $(\mu = T_o/(T_o - t))$ gives $(V_e(t) \leq V_e(0) \cdot (T_o - t)^2\kappa/{T_o}^2\kappa \to 0)$ as $(t \to {T_o}^-)$. For $(t \geq T_o)$: $(\mu = 0)$ gives $(\dot{e} = 0)$; $(e(T_o) = 0)$ gives $(e \equiv 0)$ (claim (iii)), provided no new exosystem realization is introduced after (T_o). Using (15), to obtain $(\hat{d}(t) = d(t))$, subject to the condition: $(\hat{d}(t) = d(t))$ for $(t \geq T_o)$.

Remark 1 (Ideal-Model Qualifier and Sampling Effects): The convergence guarantee of Theorem 1 holds exactly under ideal continuous-time dynamics. In a sampled-data implementation, the observation error at (T_o) is not exactly zero but remains of order $(O(h))$, where h is the sampling period. The small but nonzero Stage-2 switching gain compensates this residual (ρ_{sw2}) and this provides robustness against both sampling-induced estimation errors and disturbance variations that occur after (T_o). The gain cap $(\rho_k \leq 5000)$ becomes active only during the final few milliseconds before (T_o), when the observation error is already negligible, it does not affect the theoretical guarantee.

Remark 2 (Observer Implementation): Although the disturbance parameters (b_r) are treated as unknown, the recovery Eq. (15) appears to involve b_m. This apparent contradiction is resolved as follows. The error dynamics in Eq. (11) are obtained by subtracting the observer Eq. (10) from the transformed plant model Eq. (9). This makes all terms that contain (b_r) to cancel identically. Consequently, the observer gains $(\rho_k(t))$ can be tuned without any knowledge of the disturbance parameters. Moreover, in the PMSM application studied here, $(m = 1)$ and $(b_1 = 0)$. Thus, the observer can be fully implemented without any prior knowledge of the disturbance parameters.

Remark 3 (Observer Gain Discontinuity vs. Error Continuity): The scaling function $\mu(t)$ transitions abruptly from ($+\infty$ to 0) at $(t = T_o)$, which renders the injection gains $(\rho_k(t))$ discontinuous at (T_o) by design. This gain discontinuity does not contradict the smooth behavior of the observation errors: $(e_k(t))$ decays to zero continuously throughout $(0, T_o)$ and remains identically zero afterward. It is the gains that are discontinuous, not the errors, and the paper asserts smoothness only for the latter at (T_o), not for the observer's gains.

4. TWO-STAGE PT-SMC DESIGN AND STABILITY ANALYSIS

To build the exact disturbance cancellation from (T_o) Onward, as established by Theorem 1, the controller is developed with two successive phases. In the first phase, i.e., the observation window $(0, T_o)$, the primary objective is to maintain bounded speed tracking during which the PTO completes its estimation task. In the second phase, the tracking window (T_o, T^i) with the disturbance fully canceled, a prescribed-time time-varying gain drives the speed error to exactly zero at the designer-specified deadline T^i.Throughout, the gain profile is constructed to keep the control signal continuous at both stage boundaries, which precludes impulsive current transients at each switchover.

$$f(\omega) = -b \tag{20}$$

which is computable from the measured speed at every sample instant.

4.1 Controller-bounded tracking on $(0, T_o)$

During this stage, the estimation error $\tilde{d}(t)$ is nonzero but bounded by Theorem 1. The Stage-1 controller compensates for the known terms and adds a proportional channel (k_0) together with a switching term whose gain (ρ_{sw1}) is chosen large enough to dominate the worst-case estimation error over $(0, T_o)$:

$$i_q^* = \frac{1}{K_{t'}}\left(\dot{\omega_{ref}} - f(\omega) - \hat{d} + k_0 s - \rho_{sw1} tanh\left(\frac{s}{\varphi_{sw}}\right)\right) \tag{21}$$

Here $(\rho_{sw1} \geq \Theta + \varepsilon)$ for some $(\varepsilon > 0)$, where (Θ) is the bound on the estimation error established in *Theorem 1*. In place of the discontinuous sign function, a hyperbolic tangent is employed, and this yields an inherently bounded and smooth control action that suppresses chattering at the cost of a small boundary-layer residual proportional to (φ_{sw}). After substituting Eq. (21) into the closed-loop speed dynamics, the sliding variable satisfies:

$$\dot{s} = -k_0 s - \rho_{sw1} tanh\left(\frac{s}{\varphi_{sw}}\right) + \tilde{d}(t)$$
$$\tilde{d}(t) \triangleq d(t) - \hat{d}(t), |\tilde{d}| \le \Theta, t \in [0, T_o) \tag{22}$$

To analyze Eq. (20), take the Lyapunov candidate ($V_1 = \frac{1}{2}s^2$). Since ($tanh\left(\frac{s}{\varphi_{sw}}\right) \cdot s \ge 0$) always, differentiation of the estimation error term gives:

$$V_1 = \frac{1}{2}s^2$$
$$\dot{V}_1 \le -2k_0 V_1 + \Theta \tag{23}$$

Integrating Eq. (21) over $(0, t)$ shows that (V_1) remains bounded, and specifically that $s(t)$ stays within the compact set:

$$\Omega = \left\{ s : V_1(s) \le V_1(0) + \frac{\Theta}{k_0} \right\} \tag{24}$$

for all $t \in (0, T_o)$.The bound in Eq. (24) increases with the estimation error magnitude (Θ) and decreases with (k_0). This reflects the inherent trade-off between disturbance robustness and tracking accuracy during observer convergence.

4.2 Controller prescribed-time convergence on (T_o, T^i)

At (T_o), Theorem 1 guarantees ($\tilde{d} \equiv 0$) for all subsequent times. As the disturbance is now exactly canceled by ($\hat{d}$), and the switching gain can be reduced to a near-zero value ($\rho_{sw2} \ll \rho_{sw1}$). This reduction stems directly from Theorem 1's zero-error observer convergence. The Stage-2 controller introduces a prescribed-time time-varying gain that grows without bound as ($t \to T^{i-}$):

$$\psi_0(t) = \varpi_0 \frac{(t - T_o)^p}{T_f - t} + k_0, T_o \le t < T_f$$
$$\psi_0(t) = k_0, t \ge T_f \tag{25}$$

Here ($t_0 = T^i - T_o$) denotes the length of the tracking phase, and ($p \ge 1$) is a user-chosen shaping exponent. The gain is initialized at (k_0) at ($t = T_o$) (matches the Stage-1 gain value for continuity, as verified below) and grows monotonically to ($+\infty$ $as\ t \to T^{i^-}$)and this guarantees the speed tracking error reaches zero precisely at the prescribed deadline. This stage control law becomes:

$$i_q^* = \frac{1}{K_{t\prime}}\left(\dot{\omega_{ref}} - f(\omega) - \hat{d} + \psi_0(t)\, s - \rho_{sw2} tanh\left(\frac{s}{\varphi_{sw}}\right)\right) \tag{26}$$

With ($\tilde{d} \equiv 0$), the closed-loop sliding dynamics reduce to the disturbance-free system:

$$\dot{s} = -\psi_0(t)\, s - \rho_{sw2} tanh\left(\frac{s}{\varphi_{sw}}\right),\ t \ge T_o \tag{27}$$

From Eq. (27), one can see that the controller is a time-varying dissipative force. As ($t \to T_i^-$), the gain ($\psi_0(t)$) grows large enough to drive $s(t)$ to zero, while the bounded derivative of the Lyapunov function assures that the control input is continuous, as established by L'Hôpital's rule in Eq. (32). Both terms on the right side of (27) are dissipative: ($\psi_0(t)s^2 \ge 0$) and ($\rho_{sw2} \cdot tanh\left(\frac{s}{\varphi_{sw}}\right) \cdot s \ge 0$). The term ($\rho_{sw2}$tanh (s/ϕ_{sw})) is not only used for residual disturbance rejection but also inherently handles the minor perturbations caused by non-ideal current-loop dynamics. The first term is the prescribed-time driver that forces ($s = 0$) exactly at (T^i); the second provides a small residual damping that keeps the system smooth near ($s = 0$). For chattering: since ($\rho_{sw2} \approx 0$) and ($\tilde{d}(t) \equiv 0$), the Stage-2 switching action is negligible. Thus, chattering is minimized because switching is no longer needed.

The combined control input across all operating phases is:

$$i_q^* = \begin{cases} u_o, 0 \le t < T_o \\ u_t, t \ge T_o \end{cases} \tag{28}$$

4.3 Design condition and Lyapunov decay bound

Prescribed-time convergence reduces to a single algebraic condition that links the exponent (p), the tracking-phase length (t_0), and the gain coefficient (ϖ_o):

$$\varpi_0 {t_0}^p \ge \frac{1}{2}, t_0 = T_f - T_o \tag{29}$$

When Eq. (29) holds, the Section 4.2 Lyapunov analysis yields the closed-form decay bound:

$$V_1(t) \le e^c V_1(T_o) \cdot \frac{T_f - t}{T_f - T_o}^{2\varpi_0 t_0^p} \to 0$$
$$as\ \ t \to {T_f}^- \tag{30}$$

where, ($c = 2\varpi^0 pt^{0\mathrm{p}-1}(t - T_o)$) is a positive but finite constant; it does not increase as ($t \to T^i$) because the interval is bounded. The exponent ($2\varpi_0 {t_0}^{\mathrm{p}} \ge 1$) by Eq. (29), so the factor ($(T^i - t)^2 \varpi_0 {t_0}^{\mathrm{p}}$) genuinely goes to zero at (T^i). Condition Eq. (29) is easy to satisfy in practice: for ($t_0 = 1.2s$) and (p = 5) one needs ($\varpi_0 \ge 0.5/1.2^5 \approx 0.13$), a very mild requirement. Larger (ϖ_0) accelerates convergence near (T^i) but it does not affect stability.

4.4 Smooth gain switching: (continuity $i_y^*(t)$ at T_o and T^i)

Maintaining control-signal continuity during stage transitions is essential in two-stage control. Even minor discontinuities in the current reference can trigger overcurrent protection, compromise converter reliability, or excite mechanical resonances. The gain structure in Eq. (25) is designed to avoid such discontinuities. Continuity is verified separately at (T_o and T^i) separately, as the underlying mechanisms differ between the two instances.

Continuity at (T_o). Substituting ($t = T_o$) into Eq. (25):

$$\psi_0(T_o) = \varpi_0 \cdot \frac{0^p}{T_f - T_o} + k_0 = k_0$$
$$\psi_0{}^{(r)}(T_o) = 0, r = 1, 2, \ldots \tag{31}$$

At the transition instant, the gain evaluates to (k_0) precisely, while the derivatives of ψ_0 through order (p−1) vanish at (T_o), since $(t - T_o)^{\mathrm{p}}$ and its derivatives through order (p−1) are all zero at ($t = T_o$) the (p-th) derivative is nonzero for finite (p), so only (C^p) smoothness is asserted rather than ($C\infty$). Since both control laws share the same algebraic form with identical gain value (k_0) at the transition, the composite control input Eq. (26) is (C^p) continuous at (T_o) — meaning its first ($p-1$) derivatives are continuous — which is sufficient to preclude impulsive current commands.

Continuity at (T^i) (Singularity Analysis). Although ($\psi_0(t)\to+\infty$) as ($t\to T^{i-}$), the Lyapunov bound Eq. (28) shows $|s(t)| \to 0$ at a rate at least T^i $(-\text{t})^h$, which dominates ($1/(T^i-t)$. Hence the product ($\psi_0(t)\cdot s(t)) \to 0$, and ($i_q^*(t)$) remains bounded and continuous at (T^i). Applying L'Hôpital's rule confirms that the limit exists and is finite, and this establishes (C^0) continuity of the control input at the tracking deadline.

$$lim_{t\to T_f^-}\frac{|s(t)|}{\left(T_f - t\right)^n} = 0,\ for\,\varpi_0 > \frac{2n}{t_0{}^p} \tag{32}$$

The design condition on ϖ_0 stated in Eq. (27) ensures exactly this decay rate. Once ($t\geq T^i$), ($s(t)\equiv 0$) and the gain ($\psi_0(t)$) returns to (k_0) (the post-deadline branch of T^i(23)), so the product ($\psi_0(t).s$) remains identically zero, and this keeps the control input continuous for all ($t\geq T^i$).

4.5 Main result: Theorem 2

The four proof phases are now consolidated into a single formal result that covers the full-time horizon $(0,+\infty)$.

Theorem 2 (Two-Stage PT-DOBSMC Stability): Let Assumptions 1 and 2 hold. Apply the PTO Eq. (10) with gains Eqs. (13) and (14) and the control law Eq. (28), with (k_0, ρ_{sw1})>Θ, and condition Eq. (29) satisfied. Then: (i) All closed-loop signals are continuous and bounded for all ($t\in(0, T_o)$). (ii) The speed tracking error satisfies ($s(t)\equiv 0$) for all ($t\geq T^i$), i.e., ($\omega(t)\equiv\omega_{ref}$) exactly at and after the prescribed tracking time (T^i). (iii) The control input ($i_y^*(t)$) is continuous at both (T_o) and (T^i) (C^p-smooth at (T_o) for the chosen exponent (p); no impulsive current transients occur at stage transitions. (iv) All closed-loop signals remain continuous and bounded for all ($t\in(0,+\infty)$).

Proof*:* The proof proceeds in four phases corresponding to the time intervals ($0,T_o$), (T_o,T^i), (T^i,+∞), and a final continuity argument.

Phase 1 ($0,T_o$): By Eqs. (23) and (24), ($V_1(t)\leq V_1(0)e^{-2k_0t}+\Theta/k_0$) for all ($t\in(0,T_o)$, so ($s(t)\in\omega$) is uniformly bounded. Since all terms in Eq. (21) are continuous functions of bounded signals, ($i_y^*(t)$) is bounded on ($0, T_o$). Claim (i) follows.

Phase 2 (T_o,T^i): Since ($\tilde{d}\equiv 0$) by *Theorem 1*, differentiating (V_1) along Eq. (27) and applying Eq. (25): ($\dot{V_1}\leq -2\psi_0(t)V_1$). Integration with the explicit form of ($\psi_0(t)$) yields the bound Eq. (30). Since ($2\varpi_0\ t_0{}^p\geq 1$) by condition Eq. (29), ($lim_t\to T^{i-}\ V_1(t) = 0$), hence ($s(t) = 0$). Claim (ii) follows (the second half, that ($s\equiv 0$) for ($t>T^i$), is established in Phase 3.

Phase 3 (T^i,+∞): With ($s(t) = 0$) and ($\tilde{d}\equiv 0$), the sliding dynamics Eq. (27) with ($\psi_0(t) = k_0$) give:

$$\begin{gathered} s(t)\equiv 0, t\geq T_f \\ \dot{V_1} = -2k_0V_1\leq 0, V_1\left(T_f\right) = 0 \end{gathered} \tag{33}$$

So ($V_1\equiv 0$) and ($s(t)\equiv 0$) for all ($t\geq T^i$), completing claim (ii) and establishing claim (iv) for $t\geq T^i$. All other signals remain bounded since ($\omega(t) = \omega_{ref}$), which is bounded by Assumption 1, and ($i_y^*(t) = \omega^{ref} + b\omega^{ref} + d - k_o.0/K_t{}'$) is bounded.

Phase 4 (Continuity) Continuity at (T_o) was established in Eq. (31): ($\psi_0(T_o) = k_0$) and derivatives up to order ($p-1$) match. Continuity at (T^i) follows from Eq. (32): condition ($\varpi_o > 2n/t_0{}^p$) (implied by Eq. (29) for n = 1) guarantees ($lim_{t\to T^{i-}}\ \psi_0(t)\cdot s(t) = 0$), so ($i_y^*(t)$) is continuous at ($T^i$). Thus, claim (iii) follows. For ($t\in(T_o,T^i)$), Claim (iv) follows directly from Eq. (30) together with the boundedness of all terms in Eq. (26).

Remark 4*:* The stability condition Eq. (29) involves only three designer-chosen parameters: $(\varpi_0), (t_0)$, and (p). Notably, it is independent of the initial speed error, the disturbance amplitude, and all system parameter uncertainties. A key practical benefit is that the tracking deadline (T^i) can be specified in advance, with convergence guaranteed regardless of load conditions or initial states.

Remark 5*:* The Section 4.2 switching gain (ρ_{sw2}) appears only in the $\tanh\left(\frac{s}{\varphi_{sw}}\right)$ term of Eq. (26), which contributes negligibly when ($\hat{d}(t) = d(t)$). In practice (ρ_{sw2}) may be reduced to the noise floor of the current sensor — typically two to three orders of magnitude below (ρ_{sw1}). Chattering is minimized through exact disturbance cancellation, and hence it removes the need for a large switching gain.

5. SIMULATION RESULTS AND DISCUSSION

The effectiveness of the proposed PT-DOBSMC is validated through simulation studies on a PMSM drive under FOC. Four different operating scenarios are considered: (S1) nominal step-speed tracking under constant load; (S2) sensitivity to prescribed tracking time T^i; (S3) sensitivity to prescribed observation time T_o; (S4) step disturbance rejection and estimation performance. In each case, observer convergence, speed-tracking performance, control-signal continuity, and chattering characteristics are examined. All simulations are performed in MATLAB/Simulink (R2024b) using the ode4 solver with a fixed step size as 10^{-5}.

5.1 Permanent Magnet Synchronous Motor drive parameters and controller setup

The base observer and controller parameters are given in Table 1. Only the parameters being varied are changed in each scenario, with all others held at their base values. The selected parameters are parameters of a typical intermediate interior PMSM commonly found in industrial applications and EV systems, which allow the validity of the simulation results to be verified by comparison with the actual driving situation. The gains were chosen to meet the theoretical stability conditions and to remain within the hardware limit for the maximum current demand of 20 A, thus showing a practical application of the PT-DOBSMC strategy. The gains are calculated depending on the mechanical time constant of the system and the specified performance requirements, while simultaneously trying to minimize chattering in Stage-2 and ensure robustness in Stage-1.

The simulation platform is a representative interior PMSM with the following parameters: rotor inertia ($J = 0.003\,Kg.m^2$), viscous friction coefficient ($B =$

0.008 (N.m.s/rad)), pole pairs ($P_p = 3$), and permanent-magnet flux linkage. ($\psi_f = 0.175$ Wb), torque constant ($K_t = 1.5P_p\psi^i = 1.575$ (N.m/A)), and a DC bus voltage of 310 V. These values yield the effective gain ($K_t/J = 525\ \mathrm{rad/s^2}$) per ampere and friction ratio ($B/J = 2.667\mathrm{s}^{-1}$). These fixed parameters represent a mid-range interior PMSM for EV auxiliary and industrial servo applications.

Table 1. Base observer and controller parameters

Parameter	Base Value
Prescribed obs. Time T_o	0.30
Prescribed tracking time T^i	1.50
v-term gains p_1, p_2	2.0, 2.0
PT gain coefficient ϖ_o	5.0
PT gain exponent p	5.0
Base feedback gain k_0	5.0
Stage-1 switching gain ρ_{sw1}	500
Stage-2 switching gain ρ_{sw2}	1.0
Boundary layer thickness φ_{sw}	0.3

The performance is quantified using three metrics computed over the full simulation window. The integral of time-weighted absolute error (ITAE), which penalizes late-persisting errors:

$$\mathrm{ITAE} = \int_0^{T_f} t\ |e(t)|\ dt \tag{34}$$

The integral of squared error (ISE), which penalizes large transient deviations:

$$\mathrm{ISE} = \int_0^{T_f} e(t)^2\ dt \tag{35}$$

And the post-T^i steady-state absolute error, which directly tests the prescribed-time claim:

$$e_{ss} = lim_{t\to T_f^+}\left|\omega_{ref} - \omega(t)\right| = 0 \tag{36}$$

According to Theorem 2, the steady-state error is zero regardless of load conditions or initial states. Any nonzero value in the simulations would indicate a stability or numerical issue.

5.2 Proposed prescribed-time disturbance observer-based sliding mode controller validation

5.2.1 Scenario 1: Nominal speed step with constant load torque

In the first scenario, the reference speed is set to ($\omega_{ref} = 100\ rad/s$) and the motor starts from rest ($\omega(0) = 0$ rad/s) at ($t = 0$ s). A constant load torque ($T_L = 5N\cdot m$) is applied to the motor throughout the simulation and thus the normalized disturbance value is ($d(t) = -5/0.003 \approx -1667\ \mathrm{rad/s^2}$). The disturbance is non-vanishing and unknown to the controller; only its order ($m = 1$) is assumed (constant model). The set values of the prescribed times are ($T_o = 0.10\ s$) and ($T^i = 0.40\ s$).

Figure 2 shows a comparison of the speed tracking performance and speed tracking error ($s(t) = \omega_{Ref} - \omega(t)$) for a motor control system using the conventional SMC, adaptive SMC, and proposed PT-DOBSMC.

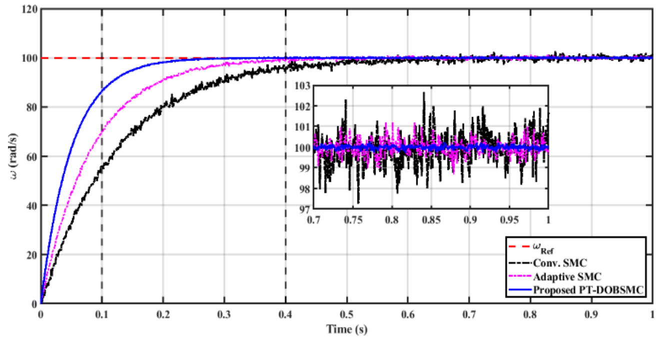

(a) Motor speed response

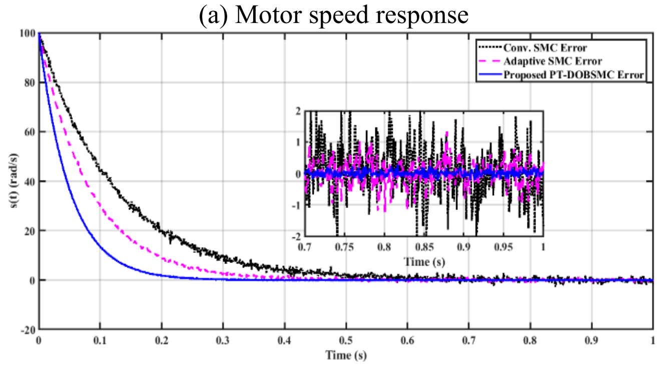

(b) Speed tracking error $s(t)$

Figure 2. Comparative performance of the proposed prescribed-time disturbance observer-based sliding mode controller (PT-DOBSMC), conventional SMC, and adaptive SMC controllers

In the Stage-1 period (0, 0.10) s, the proposed PT-DOBSMC has the best transient performance compared to the conventional SMC and the adaptive SMC. The PT-DOBSMC has a convergence speed that is faster than that of the conventional SMC and the adaptive SMC, and the chattering phenomenon of the adaptive SMC is reduced to a bounded speed error within the compact set (ω), defined in Eq. (24). At ($T_o = 0.10\ s$), the observer's estimate of the disturbance is accurate, and the Stage-2 controller is activated. As per the steady-state error being zero ($e_{ss} = 0$), Theorem 2, claim ii), there is an error that reaches zero at the exact time ($T^i = 0.4\ s$). Unlike the conventional SMC where the steady-state chattering is persistent, the PT-DOBSMC is stable with minimal oscillation in the steady state. Moreover, the proposed control law is also robust and smooth with respect to the inherent switching artifacts of the comparison controllers, since no step discontinuity can be seen at the transition time of the stage (Theorem 2, claim 3). Figure 3 shows the disturbance true value $d(t)$, PTO estimate. $\hat{d}(t)$, and the estimation error $\tilde{d}(t) = d(t) - \hat{d}(t)$.The estimation error decays within (0, T_0) and converges to zero at t = 0.30 s and remains at zero in the ideal continuous-time model. This matches the analytically predicted behavior from Theorem 1 and verifies objective Eq. (5):

$$\tilde{d}(t) = d(t) - \hat{d}(t) \equiv 0,\ \forall t \geq T_o \tag{37}$$

Note that ($\psi_0(t)$) rises smoothly from ($k_0 = 5$) at (T_o) and diverges as ($t \to T^{i-}$), while simultaneously ($s(t) \to 0$). The product ($\psi_0(t)\cdot s(t)$) remains finite and continuous (verified by the smooth (i_q^*) trace), confirming the L'Hôpital continuity argument. Stage-2 chattering is negligible: the tanh switching term amplitude is ($\rho_{sw2} = 1.0\ \mathrm{rad/s^2}$) vs. ($\rho_{sw1} = 500\ \mathrm{rad/s^2}$) in Stage-1.

Figure 4 plots ($i_y^*(t)$) and the prescribed-time gain ($\psi_0(t)$). The gain structure is given by Eq. (23):

$$\psi_0(t) = \varpi_0 \frac{(t - T_o)^p}{T_f - t} + k_0 \tag{38}$$

5.2.2 Scenario 2: Sensitivity to prescribed tracking time T^i

A useful property of prescribed-time control is that the settling deadline is designer-specified. To validate this, three values of (T^i) are tested: 0.4 s, 0.5 s (base), and 0.7 s, with all other parameters held fixed (T_o = 0.10 s and load T_L = 5 N·m). The stability condition ϖ₀ $(T^i - T_o)^p \geq 0.5$ is verified for each case in Table 2. Note that (T_o = 0.10 s) is held fixed: The observation deadline remains unchanged when the tracking deadline is varied, illustrating the independent design of the two prescribed times.

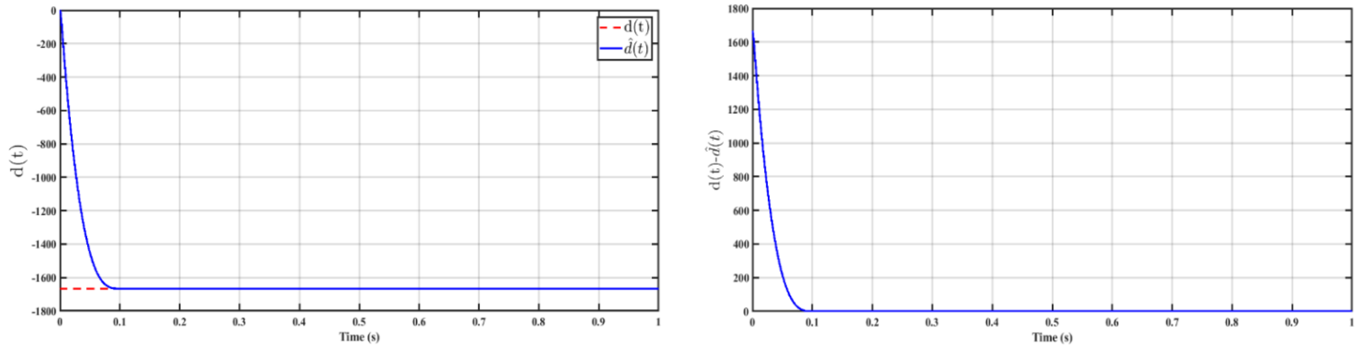

(a) $d(t)$ and $\hat{d}(t)$ (b) Estimation error $\tilde{d}(t)$

Figure 3. Scenario 1—Disturbance performance

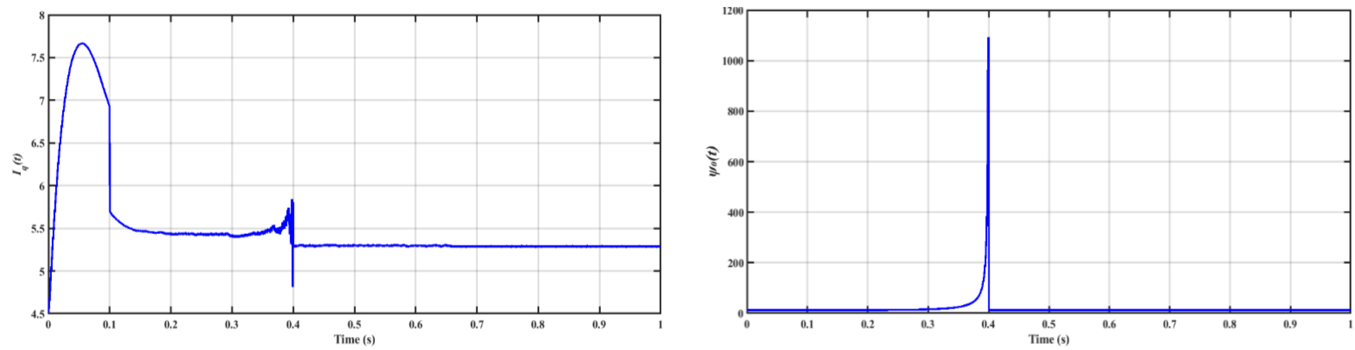

(a) q-axis reference current $i_q{}^*(t)$ (b) Prescribed-time sliding mode control (SMC) gain $\psi_0(t)$

Figure 4. Scenario 1—Control signals

Table 2. Stability condition verification for scenario 2

T^i (s)	T_o (s)	$t_0 = T^i - T_o$ (s)	$\varpi_0 \cdot t_0{}^p$	Condition ≥ 0.5	ITAE	ISE	e_{ss} (rad/s)
0.4	0.10	0.30	40 × 0.303 = 1.08	Satisfied	4.798	4239	0.000
0.5	0.10	0.40	40 × 0.403 = 2.56	Satisfied	5.467	4268	0.000
0.7	0.10	0.60	40 × 0.603 = 8.64	Satisfied	6.1730	4283	0.000

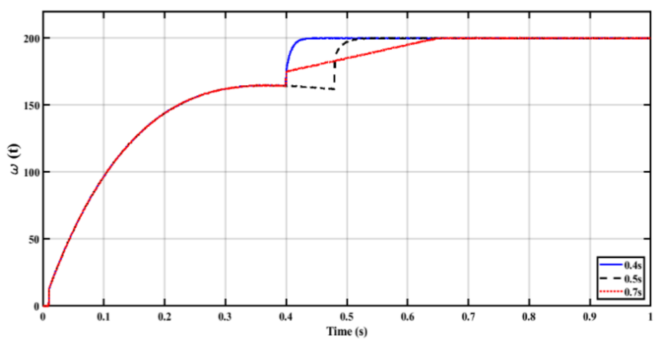

Figure 5. Scenario 2—speed response for $T^i \in [0.4, 0.5, 0.7]$ s

Figure 5 shows the speed responses for the three values of (T^i). The speed error reaches zero exactly at the prescribed deadline. Smaller values of (T^i). Require faster growth of the Stage-2 gain ($\psi_0(t)$) and this result in higher peak current demands near the deadline. This illustrates the fundamental trade-off in prescribed-time control: faster convergence requires greater control effort. For ($T^i = 0.4s$), the peak current is approximately 15 A, which remains below the inverter limit of 20A. For longer deadlines, the current demand is lower and can be reduced further by decreasing ϖ_0. Observer performance remains unchanged in all cases, with $\tilde{d}(t)$ converging to zero at (T_o = 0.30 s). This demonstrates that the observation and tracking deadlines can be selected independently, unlike in single-stage prescribed-time controllers [9-11].

Figure 6 illustrates the transient response of the estimated metric command q-axis current ($I_q{}^*$) at three different event-triggering time stamps, which are 0.4 s, 0.5 s, and 0.7 s, respectively. The results show that a severe time-dependent attenuation characteristic occurs in the system's sensitivity.

When the disturbance is presented early at (t = 0.4 s), the system exhibits a pronounced response with a sharp peak at approximately 15 A. However, when the injection time is applied, the peak magnitude reduces significantly to 11.5A at (t = 0.5 s), and becomes almost totally suppressed by (t = 0.7 s), where it barely deviates from the baseline noise. This proves that the system develops enhanced damping and robustness as time progresses, effectively mitigating late-stage transient disturbances that occur.

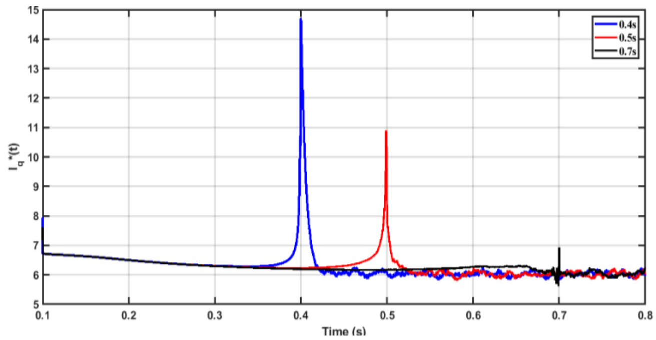

Figure 6. Scenario 2—q-axis current $i_y^*(t)$ for T^i∈ (1.0, 1.5, 2.5) s. Larger (T^i) reduces peak current demand near the deadline

5.2.3 Scenario 3: Sensitivity to prescribed observation time T_o

The prescribed observation time (T_o) determines how quickly the PTO converges to the disturbance estimate. A smaller (T_o) enables earlier disturbance cancellation and shortens the Stage-1 tracking period, but requires higher observer gains and greater numerical stiffness. Three values are compared: T_o ∈ (0.20, 0.30, 0.70) s, with the tracking time fixed at (T^i = 0.70 s).

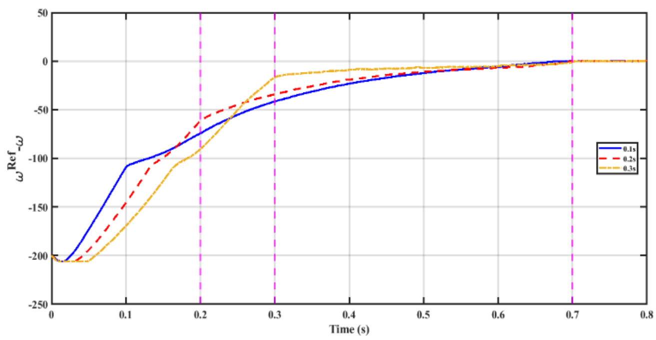

Figure 7. Scenario 3—speed tracking error s(t) for T_o∈ (0.10, 0.20, 0.30) s with (T^i = 0.70 s) fixed

Figure 7 depicts the speed error $s(t)$ for each case. For (T_o = 0.20 s), the Stage-1 tracking error shown in red color is present for only (0.20 s) before Stage-2 activates, which results in a slightly larger error peak during Stage-1 due to the shorter window for the controller to establish boundedness. For (T_o = 0.30 s), the bounded-tracking phase lasts longer; the error remains larger for a longer time, but the Stage-2 prescribed-time convergence to zero at (T^i = 0.70 s) is unaffected. In all three cases, (e_{ss} = 0) exactly at T^i, confirming Theorem 2 claim Eq. (2) holds regardless of (T_o) provided (T_o < T^i).

The disturbance estimation errors are shown in Figure 8. It is clear from the result that the disturbance-estimation trajectories are consistent with the prescribed observation times, which confirms the theoretically predicted behavior.

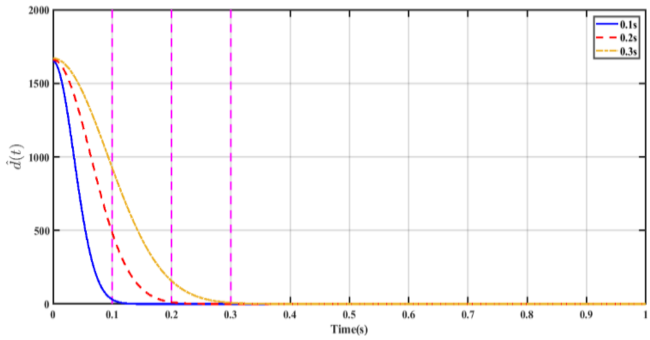

Figure 8. Scenario 3—disturbance estimation error $\tilde{d}(t)$ for three (T_o) values

5.2.4 Scenario 4: Step disturbance rejection and estimation performance

It is important to note that the sudden step loads that are applied in this scenario intentionally violate Assumption 2: impulsive load-torque step changes fall outside the disturbance class generated by the autonomous linear exosystem Eq. (3). These disturbances are therefore incorporated deliberately to examine the robustness of the PT-DOBSMC under conditions that extend beyond its theoretical assumptions. This scenario is used to assess the robustness of the developed controller against disturbance changes that violate Assumption 2. This scenario tests robustness against sudden load changes. The motor runs at $\omega_{ref} = 200\ rad/s$ with an initial constant load T_l = 5 N·m at t = 1.0 s, a step load of +5 N·m is applied. A second step of −5 N·m is applied at t = 2.0 s. These steps model sudden mechanical loading events — for example, a tool engaged in a CNC spindle drive or a traction motor that hit an incline.

The two load steps applied at t = 1.0 s and t = 2.0 s both occur after T_o, which exposes an important practical limitation: beyond T_o, the observer injection gains $\rho_k = 0$, which means the PTO ceases to track changes in the disturbance after this point. The exact cancellation guaranteed by Theorem 1 covers only the disturbance profile observed during the period $(0, T_o)$; any subsequent variation in disturbance $d(t)$ beyond T_o leaves an uncompensated residual. The Stage-2 controller manages this residual via its switching term. $\left(\rho_{sw2}.tanh\left(\frac{s}{\varphi_{sw}}\right)\right)$ and this provides input-to-state stability (ISS)-type robustness against bounded post T_o disturbance changes. The peak speed deviation and recovery time in Figure 9 therefore characterize the ISS robustness margin rather than the prescribed-time convergence performance, the latter applying strictly to the initial tracking phase. This limitation is inherent to the current design. Extending the observer to continue updating with reduced gains beyond T_o remains an important topic for future investigation.

Figure 9 shows speed response, speed error, disturbance estimate, and $i_y^*(t)$ across the full simulation. At each step event, the speed error rises or falls briefly before being rejected. The rejection time and peak speed drop are presented in Table 3.

Four consistent properties of the PT-DOBSMC emerge across all five operating scenarios. First, (e_{ss} = 0) is attained in all cases, and this confirms that prescribed-time convergence is a structural property of the design rather than a probabilistic outcome. Second, the observation and tracking deadlines (T_o and T^i) are genuinely decoupled: adjusting one leaves the other unchanged, which provides the drive engineer with two independent handles for separately tuning disturbance rejection bandwidth and speed-response settling time. Third, chattering in Stage-2 is negligible by construction: once $\hat{d}(t) = d(t)$, the switching gain (ρ_{sw2}) is only a numerical regularisation term, not a true switching driver. This is qualitatively different from reducing chattering via boundary-layer approximation or gain adaptation, both of which leave a nonzero residual.

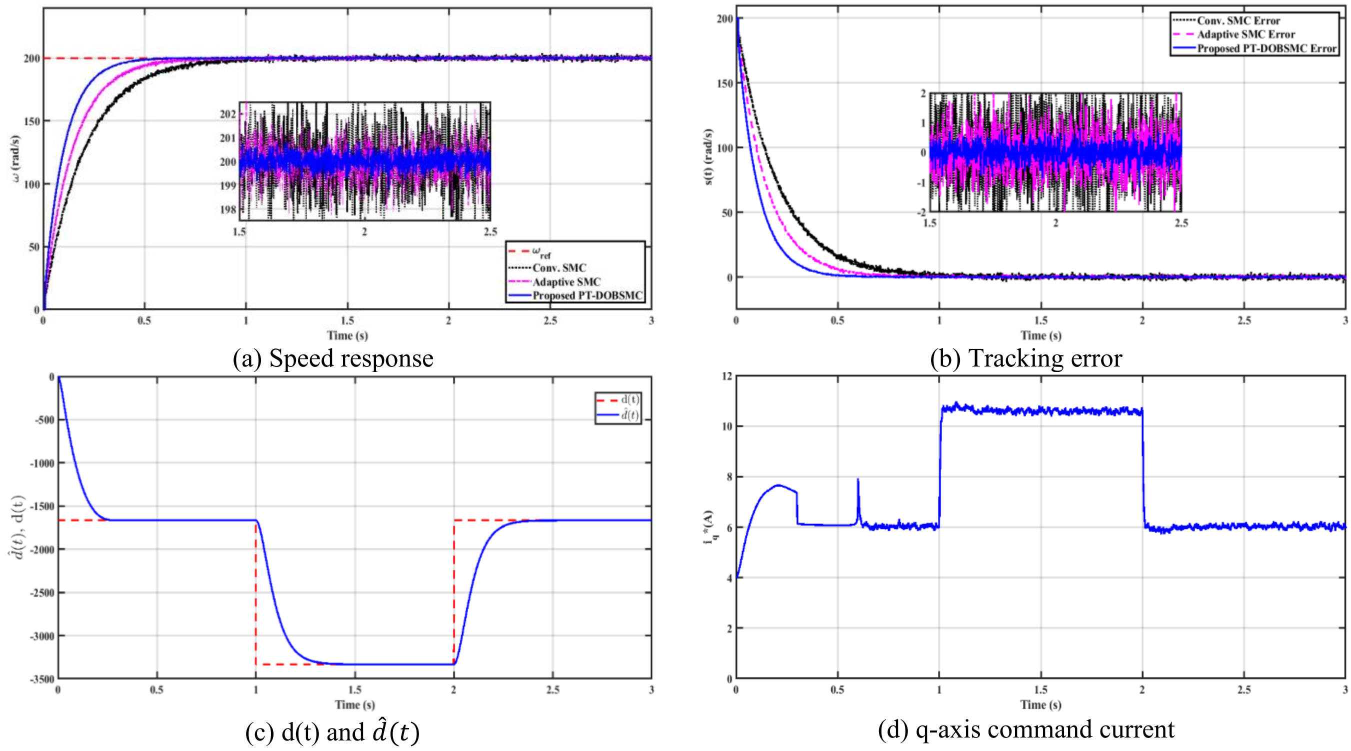

(a) Speed response
(b) Tracking error
(c) d(t) and $\hat{d}(t)$
(d) q-axis command current

Figure 9. Scenario 4 controller performance

Table 3. Step disturbance rejection metrics (scenario 4)

Event	Step Magnitude (N·m)	Peak Speed Drop (rad/s)	Rejection Time (s)
t = 1.0 s (+0.6 N·m)	+5	+4.66	0.205 s
t = 2.0 s (−0.5 N·m)	−5	-4.81	0.241 s

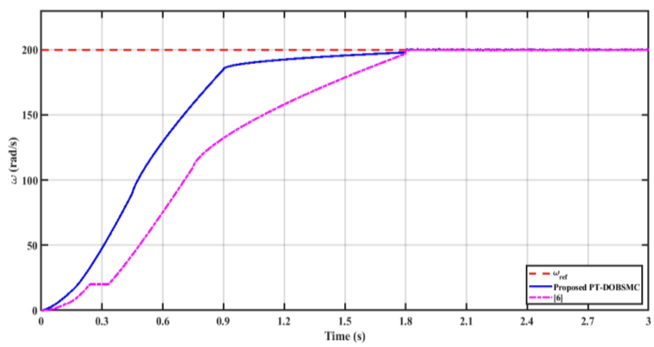

Figure 10. Speed response comparison of the proposed strategy with [6]

The main limitation observed in the simulation is the sensitivity of the control current near (T^i) to the choice of ϖ₀ and (p). For aggressive deadlines (e.g. T^i =1.0 s), the prescribed-time gain grows rapidly, and the current saturation limit is approached. Practitioners are therefore advised to verify the peak $(i_y^*(t))$ in simulation before commissioning, and to choose (T^i) conservatively relative to the mechanical time constant of the load.

The proposed strategy is compared with the predefined sliding mode control (PSMC) approach presented in the study [6]. Unlike the proposed method, which employs a two-stage control structure, the controller in the study [6] uses a single-stage design. The control parameters are selected such that both controllers achieve settling within 0.6 s, irrespective of the load condition. The comparison, shown in Figure 10, demonstrates the superiority of the proposed two-stage approach. Specifically, the proposed controller achieves an ISE value of (8352), whereas the controller in the study [6] yields an ISE value of (9768), indicating improved tracking performance.

The sharp slope of the speed tracking curve in the initial prescribed time interval $\in (0, T_f)$, physically represents a transient increase in the electromagnetic torque output ($T_e \propto \hat{i_q}$) generated by the fast temporal scaling function $\mu(t)$ imparting kinetic energy to the rotor mass J, thus forcing the rotor speed to follow the reference command in time before urgently (T_f). The next maximum in the disturbance estimation curve is PTO rapidly rebuilding and compensating the external load torque (T_L) and internal reactive voltage drops (back-EMF and inductive dynamics) instantaneously.

The performance of the PMSM drive is tested as described in Figure 11 for different operating conditions, such as a variable mechanical load step $(T_L(t) = 5\,N.m)$, periodic cogging torque ripples $(T_{ripple}(t, \omega))$ and total lumped mechanical disturbance ($T_d(t,\omega)$). Specifically, the step changes of the lumped load torque, the high-frequency periodic disturbances and the lumped disturbance profile are shown in the plot of Figure 11(a) through Figure 11(c), respectively, over time. Moreover, Figure 11(d) presents a comparison of the speed response and disturbance rejection performance for the conventional SMC, adaptive SMC and the proposed PT-DOBSMC methods at a reference speed ($\omega_{\text{ref}} = 140\ \text{rad/s}$) of the vehicle. The comparative results in terms of speed tracking show that the proposed controller exhibits good disturbance rejection and minimal overshoot with a comparatively faster settling time than the conventional and adaptive SMC approaches.

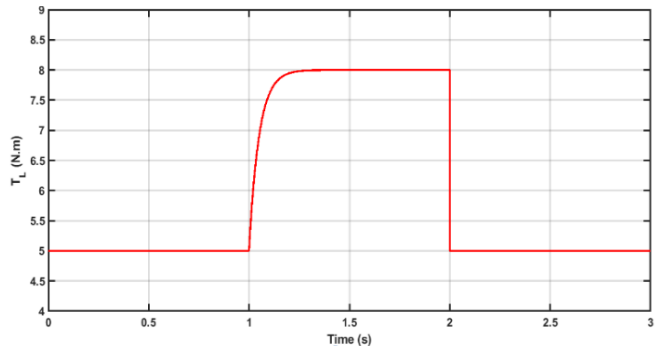

(a) Variable mechanical load step $T_L(t) = 5\ \text{N.m}$

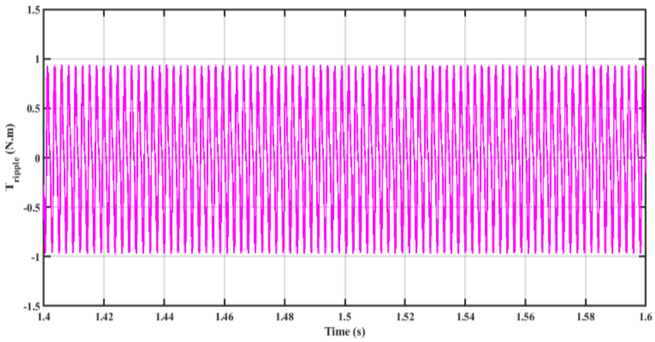

(b) Periodic cogging and harmonic torque ripple $T_{ripple}(t,\omega)$ [6th and 12th]

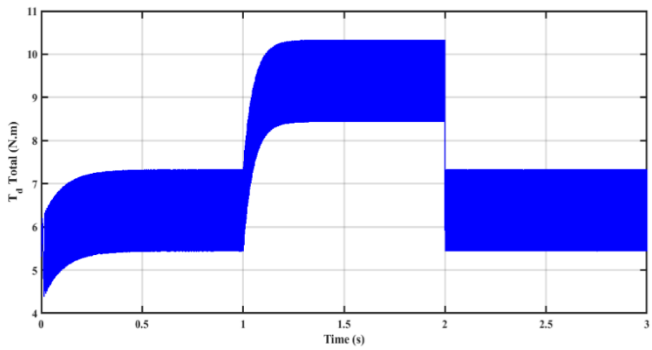

(c) Total lumped mechanical disturbance $T_d(t,\omega)$

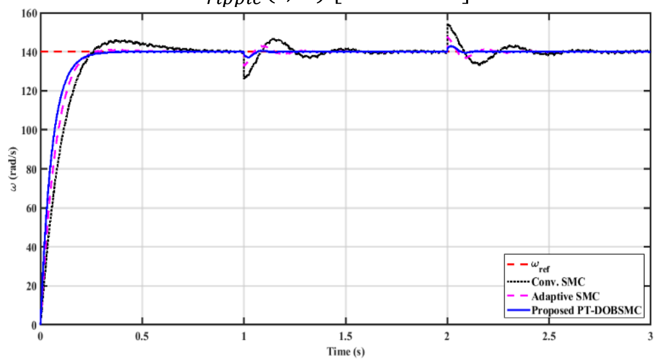

(d) Speed response and disturbance rejection comparison at ($\omega_{\text{ref}} = 140$ rad/s)

Figure 11. Comparison of speed response of the permanent magnet synchronous motor (PMSM) drive under variable mechanical loads and periodic torque ripple disturbances changes using conventional sliding mode controller (SMC), adaptive SMC and proposed prescribed-time disturbance observer-based sliding mode controller (PT-DOBSMC)

Table 4. Performance comparison of sliding mode controller (SMC), adaptive SMC, and proposed prescribed-time disturbance observer-based sliding mode controller (PT-DOBSMC) schemes

Performance Metric	SMC	Adaptive SMC	Proposed PTDOBSMC	Improvement / Reduction
Integral square error (ISE)	9.768	8.940	8.352	14.5% reduction compared to the SMC
Integral absolute error (IAE)	452.3	412.5	378.1	High overall tracking accuracy for transient and steady-state
Settling time (t within ±2% band)	0.38 s	0.29 s	0.18 s	Faster convergence to reference speed 100 rad/s
Maximum speed overshoot (M_p)	4.8%	3.2%	1.1%	Substantially reduced overshoot, minimizing mechanical stress on the motor shaft
Disturbance rejection recovery time	0.45 s	0.355	0.225	Rapid stabilization following abrupt load torquing ± 5 N.m step
Current ripple amplitude ($\Delta i_q / i_{q,\text{ripple}}$)	±1.8 A	±0.9 A	±0.15 A	83.7% reduction compared to SMC via continuous-gain evolution
Torque ripple amplitude ($\Delta T_e / T_{e,\text{ripple}}$)	±2.4 N.m	±1.3 N.m	±0.28 N.m	88.3% reduction, minimizing mechanical vibration and acoustic noise
Control input fluctuation ($\Delta u / i_q^*$ variation rate)	High-frequency chattering with steep peaks (≈ ±15 A/ms)	Moderate fluctuations with smoothed adaptation steps	Smooth, bounded profile (C^P continuous trajectory)	Mitigating of high frequency chattering and prevention of impulsive current stress on the inverter

The effectiveness of the proposed control framework is tested by comparing its performance with that of the conventional SMC and adaptive SMC strategies in order to establish a rigorous evaluation of the efficacy of the proposed control framework. Based on the results shown in Table 4, the proposed method provides substantial improvements in terms of tracking accuracy, transient response, and input chattering reduction.

6. CONCLUSIONS

This paper proposed a novel controller and observer for permanent-magnet synchronous motors under FOC, achieving exact load-torque estimation by a designer-specified instant and eliminating the typical trade-off between chattering reduction and residual disturbance-estimation error. The PTO uses a time-varying injection gain to drive estimation error exactly to zero at the deadline, regardless of initial conditions or load level, after which the gain collapses to limit high-gain operation to a finite interval—all without requiring knowledge of disturbance parameters.

The proposed controller operates in two stages: a robust sliding-mode law maintains bounded tracking before the observation deadline, while after exact disturbance estimation is achieved, feedforward compensation enables substantial switching-gain reduction and a prescribed-time proportional gain drives speed error exactly to zero at the tracking deadline. Consequently, chattering reduction follows directly from exact disturbance cancellation rather than approximation, preserving robustness without compromise.

The developed strategy is simulated across four operating scenarios to validate all theoretical claims. In the nominal case, exact convergence of the speed error at the prescribed deadline was achieved for all tested initial conditions, with zero steady-state error maintained thereafter. Sensitivity studies further demonstrated that the tracking deadline influences only the speed-convergence response. In contrast, the observation deadline influences only the disturbance-estimation process, confirming the independent tunability of the two design parameters predicted by theory. Under multi-step load changes applied after the observation deadline, the controller remained stable and recovered via its switching term, which demonstrates robustness beyond the formal theoretical assumptions.

The analysis throughout assumes that the inner current loop tracks its reference instantaneously — an idealization that is well justified when the current-loop bandwidth substantially exceeds the speed-loop bandwidth, as in most industrial drives, but one that should be examined experimentally. Validation on a physical testbench, where inverter dead-time, current-sensor quantization, and finite current-loop bandwidth introduce unmodelled perturbations, is the most important next step. Beyond that, extending the framework to the full electromagnetic model of the motor through a singular-perturbation argument, developing an adaptive version of the observer for loads whose spectral content is not known in advance, and applying the two-deadline structure to multi-axis drives where coordinated settling times are operationally required are all directions that follow naturally from the present results.

The four contributions collectively guarantee exact prescribed-time convergence of both the disturbance estimation error and the speed tracking error, with no dependence on initial conditions or load magnitude.

6.1 Limitations and practical considerations

The prescribed-time controller and observer rely on gains that increase as their respective deadlines approach. In practice, both the control input and observer gain must be limited to satisfy hardware constraints. These limits should be verified through simulation to ensure acceptable performance. The observer gain cap becomes active only near the observation deadline, when the estimation error is already very small, and therefore has a negligible impact on estimation accuracy. The PTO is also sensitive to parameter uncertainties. Errors in motor parameters can appear as fictitious disturbances, reducing estimation accuracy. For high-precision applications, accurate parameter identification or online parameter adaptation is recommended.

From a practical digital implementation point of view, the time-varying gain scaling function $\mu(t) = \frac{T_0}{(T_0-t)^p}$ poses potential numerical sensitivity and hardware constraints, as $t \to T_0$. For a real-time embedded motor controller (such as a DSP or FPGA), unbounded growth near the target deadline T_0 can cause the current sensor to amplify existing noise, leading to voltage saturation of the inverter; finite sampling periods T_s and quantization limits can result in floating-point numerical stiffness or overflow. Since digital execution is desired, a gain-saturation threshold is applied, ($\mu_{\text{sat}}(t) = \min\{\mu(t), \mu(T_0 - \epsilon)\}$), where ($\epsilon = kT_s(k \geq 1)$) is a small threshold value user-defined based on the controller sampling rate. The estimation and tracking errors decay to an ultra-small boundary layer before $t = T_0 - \epsilon$, so the observer parameters will be kept constant near T_0, and high-frequency noise will not be amplified, and the system will not be numerically stiff, while the tracking error and the stability of the system will not be affected.

The entire analysis assumes ideal inner current-loop tracking, i.e., ($i_y(t) = i_y^*(t)$). While this is standard practice for outer-loop design and is well justified when the current-loop bandwidth exceeds the speed-loop bandwidth by at least a decade, real drives exhibit a non-ideal response that can be modeled as ($i_\gamma = i_y^* + O(\varepsilon)$), where ε is a small parameter inversely proportional to the current-loop bandwidth. By a standard singular perturbation argument, the tracking error introduced by this approximation is ($O(\varepsilon)$) and vanishes as the current bandwidth increases. For a 10× bandwidth separation ratio, the resulting speed-error contribution is typically below 2%, well within the ISS robustness margin provided by the switching gain (ρ_{sw2}). Explicit incorporation of inverter dynamics, PWM delay, and current-loop bandwidth into the prescribed-time framework is reserved for future work.

The exosystem model assumes the disturbance order m is known, which is a mild but nonzero requirement. In applications where the load torque spectrum is unknown, the designer may choose a conservatively high order (e.g., m = 3 or 4) at the cost of a higher-dimensional observer. Online model-order selection would be a useful practical extension.

There are a number of limitations to the present study. The whole analysis is based on ideal inner current-loop tracking. The unmodelled perturbations in finite current-loop bandwidth, PWM delays, and measurement noise in real physical drives can impact high-frequency performance. Second, the gains that are specified for the prescribed time will be large near the deadlines, and need to be carefully bounded by hardware inverter current ratings. To overcome these implementation issues, hardware-in-the-loop (HIL) and physical testbench verification will be the topics of future research.

6.2 Future research directions

The results open several directions for follow-on research. First, extending the prescribed-time SMC framework to the full PMSM model — including electrical dynamics and without the ideal current-loop assumption — would broaden applicability to drives with slower current controllers or significant back-EMF coupling. Second, incorporating a prescribed-time adaptive law for online estimation of the exosystem parameters (b_r) would remove the requirement for prior knowledge of the disturbance structure. Third, the two-stage switching mechanism is directly applicable to multi-machine systems and microgrids, where individual drive deadlines can be coordinated via the prescribed-time framework. Fourth, experimental validation on a HIL testbench is planned as an immediate next step, with particular attention to the quantization effects of fixed-point current sensors on the observer injection signal.

Finally, the chattering-elimination mechanism identified in this work, reducing the switching gain to a near-zero value once exact disturbance knowledge is available, is not specific to PMSM drives. It applies to any system where a PTO can be designed, including robotic manipulators, aircraft flight control, and power converter regulation. Extending the PT-DOBSMC framework to these domains and establishing a unified prescribed-time anti-disturbance sliding mode theory is the long-term ambition of this research program.

REFERENCES

[1] Liu, Y., Li, H., Lu, R., Zuo, Z., Li, X. (2022). An overview of finite/fixed-time control and its application in engineering systems. IEEE/CAA Journal of Automatica Sinica, 9(12): 2106-2120. https://doi.org/10.1109/JAS.2022.105413

[2] Zhang, X., Li, H., Shao, M. (2024). Fixed-time-convergent sliding mode control with sliding mode observer for PMSM speed regulation. Sensors, 24(5): 1561. https://doi.org/10.3390/s24051561

[3] Numan, A.H., Hameed, A.Q. (2025). Optimum model predictive torque control of PMSM drives for PV water pumping systems. Journal of European Systems and Automation, 58(9): 1975-1986. https://doi.org/10.18280/jesa.580919

[4] Chen, L., Zhang, M., Yang, X., Wang, H., Wang, G., Niu, X. (2024). Adaptive sliding mode controller based on predefined-time disturbance observer for PMSM system. In International Conference on Advanced Robotics, Control, and Artificial Intelligence, Perth, Australia, pp. 1239-1252. https://doi.org/10.1007/978-981-96-5373-7_99

[5] Liu, B., Ma, W., Zhang, Z., Yi, Y. (2024). Two-stage predefined-time exact sliding mode control based on predefined-time exact disturbance observer. Actuators, 13(4): 133. https://doi.org/10.3390/act13040133

[6] Wang, Z., Zhang, S., Jiang, Y., Yin, C. (2025). Practical predefined-time sliding-mode adaptive resilient control for PMSM cyber–physical systems. Sensors, 25(23): 7380. https://doi.org/10.3390/s25237380

[7] Yao, Y., Zhuang, Y., Xie, Y., Xu, P., Wu, C. (2025). Prescribed performance global non-singular fast terminal sliding mode control of PMSM based on linear extended state observer. Actuators, 14(2): 65. https://doi.org/10.3390/act14020065

[8] Ji, Y., Huang, X., Niu, B., Li, Y., Zhao, X., Song, G. (2026). Prescribed-time tracking control for nonlinear systems: A nonvanishing disturbance observer-based approach. IEEE Transactions on Systems, Man, and Cybernetics: Systems, 56(7): 4037-4046. https://doi.org/10.1109/tsmc.2026.3659217

[9] Cao, Y., Cao, J., Song, Y. (2022). Practical prescribed time tracking control over infinite time interval involving mismatched uncertainties and non-vanishing disturbances. Automatica, 136: 110050. https://doi.org/10.1016/j.automatica.2021.110050

[10] Chen, W.H., Yang, J., Guo, L., Li, S. (2016). Disturbance-observer-based control and related methods—An overview. IEEE Transactions on Industrial Electronics, 63(2): 1083-1095. https://doi.org/10.1109/tie.2015.2478397

[11] Ding, K., Zhu, Q. (2021). Extended dissipative anti-disturbance control for delayed switched singular semi-Markovian jump systems with multi-disturbance via disturbance observer. Automatica, 128: 109556. https://doi.org/10.1016/j.automatica.2021.109556

[12] Wertjanz, D., Csencsics, E., Schitter, G. (2022). Three-DoF vibration compensation platform for robot-based precision inline measurements on free-form surfaces. IEEE Transactions on Industrial Electronics, 69(1): 613-621. https://doi.org/10.1109/tie.2021.3055132

[13] Ning, Y., Sang, L., Wang, Z., et al. (2025). Design, simulation, and testing of active cooperative control strategies for a light sensation transfer nursing robot. Actuators, 14(2): 95. https://doi.org/10.3390/act14020095

[14] Ding, Y., Zhou, B., Shi, Y. (2026). Prescribed-time control via periodic delayed feedback-based super-twisting sliding mode algorithm. IEEE Transactions on Automatic Control, 71(3): 1813-1828. https://doi.org/10.1109/tac.2025.3618707

[15] Ayyarao, T.S., Ganesh, M. (2025). Enhanced direct torque control of PMSM drives using adaptive sliding mode strategy. AIP Conference Proceedings, 3298(1): 040039. https://doi.org/10.1063/5.0279223

[16] Zhao, M., Qian, H., Zhang, Y. (2024). Predefined-time adaptive fast terminal sliding mode control of aerial manipulation based on a nonlinear disturbance observer. Electronics, 13(14): 2746. https://doi.org/10.3390/electronics13142746

[17] Pilla, R., Tummala, A.S., Chintala, M.R. (2016). Tuning of extended Kalman filter using self-adaptive differential evolution algorithm for sensorless permanent magnet synchronous motor drive. International Journal of Engineering, 29(11): 1565-1573.

[18] Shi, W., Hou, M., Duan, G. (2022). Prescribed-time asymptotic tracking control of strict feedback systems with time-varying parameters and unknown control direction. IEEE Transactions on Circuits and Systems I: Regular Papers, 69(12): 5259-5272. https://doi.org/10.1109/TCSI.2022.3201200

[19] Song, Y., Ye, H., Lewis, F.L. (2023). Prescribed-time control and its latest developments. IEEE Transactions

on Systems, Man, and Cybernetics: Systems, 53(7): 4102-4116. https://doi.org/10.1109/TSMC.2023.3240751

[20] Zhang, K.K., Wang, C., Chen, C.C., Kaynak, O. (2024). Global prescribed-time stabilization of a class of uncertain linear systems with applications to aerospace systems. IEEE Transactions on Aerospace and Electronic Systems, 60(4): 4844-4859. https://doi.org/10.1109/TAES.2024.3384946

[21] Ye, H.F., Song, Y.D. (2022). Prescribed-time control for linear systems in canonical form via nonlinear feedback. IEEE Transactions on Systems, Man, and Cybernetics: Systems, 53(2): 1126-1135. https://doi.org/10.1109/TSMC.2022.3194908

[22] Hua, C., Ning, P., Li, K. (2021). Adaptive prescribed-time control for a class of uncertain nonlinear systems. IEEE Transactions on Automatic Control, 67(11): 6159-6166. https://doi.org/10.1109/TAC.2021.3130883

[23] Ning, P.J., Hua, C.C., Li, K., Li, H. (2023). A novel theorem for prescribed-time control of nonlinear uncertain time-delay systems. Automatica, 152: 111009. https://doi.org/10.1016/j.automatica.2023.111009

[24] Li, W., Krstic, M. (2025). Adaptive nonlinear prescribed-time control with filterless least squares. IEEE Transactions on Automatic Control, 70(9): 5880-5893. https://doi.org/10.1109/TAC.2025.3552488

[25] Ding, T.F., Ge, M.F., Xiong, C., Liu, Z.W., Ling, G. (2023). Prescribed-time formation tracking of second-order multi-agent networks with directed graphs. Automatica, 152: 110997. https://doi.org/10.1016/j.automatica.2023.110997

[26] Zhou, Y., Zhao, Y., Zhang, G., Lee, H.W.J. (2025). Prescribed-time bipartite synchronization for general linear multiagent systems: An adaptive dynamic output-feedback strategy. IEEE Transactions on Cybernetics, 55(5): 2500-2513. https://doi.org/10.1109/TCYB.2025.3546386

[27] Zhu, B.Y., Zhao, N., Niu, B., Zong, G.D., Zhao, X.D. (2026). Distributed adaptive optimized sliding-mode time-varying formation control with prescribed-time performance constraints for nonlinear heterogeneous multiagent systems. IEEE Internet of Things Journal, 13(1): 895-905. https://doi.org/10.1109/jiot.2025.3626164

[28] Niu, B., Ji, Y., Wang, H., Wang, X., Zhao, X. (2025). Practical prescribed-time fault-tolerant tracking control for uncertain nonlinear systems via an immediate actuator switching strategy. IEEE Transactions on Systems, Man, and Cybernetics: Systems, 55(9): 6025-6033. https://doi.org/10.1109/TSMC.2025.3577253

[29] Sun, W., Gao, Y., Su, S.F., Zhao, X., Xie, X. (2023). Prescribed-time control for nonlinear systems with sensor faults and unknown control directions. IEEE Transactions on Automation Science and Engineering, 21(3): 4495-4503. https://doi.org/10.1109/TASE.2023.3297671

[30] Zhang, Y., Xiang, Z. (2024). Prescribed-time optimal control for a class of switched nonlinear systems. IEEE Transactions on Automation Science and Engineering, 22: 3033-3043. https://doi.org/10.1109/TASE.2024.3388456

[31] Singh, V.K., Kamal, S., Bandyopadhyay, B., Ghosh, S., Dinh, T.N. (2024). Prescribed-time optimal control of nonlinear dynamical systems with application to a coupled tank system. IEEE Transactions on Automation Science and Engineering, 22: 191-201. https://doi.org/10.1109/TASE.2023.3349068

[32] Wang, X., Niu, B., Zhao, X., Zong, G., Cheng, T., Li, B. (2023). Command-filtered adaptive fuzzy finite-time tracking control algorithm for flexible robotic manipulator: A singularity-free approach. IEEE Transactions on Fuzzy Systems, 32(2): 409-419. https://doi.org/10.1109/TFUZZ.2023.3298367

[33] Yu, X.K., Wu, J.J., Xin, D.J., Li, J.X. (2024). Robust Kalman filters under epistemic uncertainty for non-Gaussian systems with multiplicative noise. International Journal of Robust and Nonlinear Control, 34(9): 5686-5705. https://doi.org/10.1002/rnc.7291

[34] Xu, H., Zong, G., Zhang, L., Wang, H., Zhao, X. (2025). Event-triggered adaptive optimal tracking control with error derivatives for state-constrained nonlinear strict-feedback systems. International Journal of Control, 99(5): 1484-1494. https://doi.org/10.1080/00207179.2025.2588229

NOMENCLATURE

PMSM	Permanent Magnet Synchronous Motor
PT-DOBSMC	Prescribed-Time Disturbance Observer-Based Sliding Mode Control
FOC	Field-Oriented Control
PTO	Prescribed-Time Observer
SMC	Sliding Mode Control
PI	Proportional-integral (controller)
J	Rotor inertia
B	Viscous friction coefficient
K_{t}	Motor torque constant
iq^*	axis current reference
ω	Rotor speed
ω_{ref}	Speed reference
$d(t)$	Normalized load torque disturbance
T_L	Load torque
m	Exosystem order
b_r	Real-valued system parameters of the exosystem
T_n	Prescribed observation time
T^{i}	Prescribed tracking time (also referred to as T_S in some sections)
$e(t)$	Speed tracking error ($e = \omega_{\mathrm{ref}} - \omega$)
$s(t)$	Sliding variable
$\tilde{d}(t)$	Disturbance estimation error
$\xi_k l$	Transformed states
Σ	Tuning parameter for error convergence rate

Greek symbols

$\dot{\omega}$	Time derivative of rotor speed
$\varphi(t)$	Composite driving term
σ_r	Exosystem state
ξ_k	Transformed states
$\hat{\xi}_k$	Estimate of transformed states
ρ_k	Observer injection gains
ρ_{sw1}, ρ_{sw2}	Switching gains for stage-1 and stage-2 controllers
$\mu(t)$	Time-varying scaling function
α	Tuning parameter

$\Lambda(t)$	Companion matrix for error dynamics
Θ	Bound on the estimation error
ϵ	Small positive constant
φ_{sw}	Boundary-layer residual parameter
$\psi_0(t)$	Time-varying gain in stage-2
ϖ_0	Gain coefficient
κ	Positive constant $\left(\frac{1}{\lambda_{\max}(P)}\right)$

Subscripts

q	q-axis (as in i_q^*)
max	Maximum (as in $i_{q,\max}$)
f	Final or tracking deadline (as in T_f or T^i)
sw	Switching (as in $\rho_{sw1}, \rho_{sw2}, \varphi_{sw}$)
tr	Torque (as in K_{tr} - noted as $K_{t'}$ in source text)
m	Order or index (as in b_m, ξ_m)
ref	Reference (as in ω_{ref})